Scanning Electron Microscopy

Volume 1986
Number 1 *Part I*

Article 4

3-28-1986

Signal Generation and Contrast Mechanisms in Scanning Electron Acoustic Microscopy

N. Kultscher
Universität Duisburg

L. J. Balk
Universität Duisburg

SCANNING ELECTRON MICROSCOPY/1986/I (Pages 33-43)
SEM Inc., AMF O'Hare (Chicago), IL 60666-0507 USA

0586-5581/86$1.00+05

SIGNAL GENERATION AND CONTRAST MECHANISMS IN SCANNING ELECTRON ACOUSTIC MICROSCOPY

N. Kultscher and L.J. Balk

Universität Duisburg, Fachgebiet Werkstoffe der Elektrotechnik
Leiter: Prof. Dr.-Ing. E. Kubalek
Kommandantenstraße 60, D 4100 Duisburg 1, F.R.G.

(Received for publication February 07, 1985, and in revised form March 28, 1986)

Abstract

In scanning electron acoustic microscopy (SEAM) until now the signal generation is explained mainly by an intermediate production of thermal waves. Though this so-called thermal wave approach has proven to give realistic results for metals, from experimental evidence it seems to fail for other material groups such as ceramics, dielectrics, piezoelectrics and semiconductors. As these material groups are of major technological importance, it is necessary to develop theories which help interpreting those SEAM micrographs obtained for these types of material.

In a comparative manner three different models are discussed in this paper, the well known thermal coupling, the piezoelectric coupling and the excess carrier coupling. The relevant parameters for the signal formation are determined and the contrasts achieved in electron acoustic micrographs explained by means of these models. The experimental evidence discussed for all important material groups supports the three models significantly, and the results obtained can be interpreted quantitatively in terms of material properties and primary electron beam parameters.

KEY WORDS: Scanning electron acoustic microscopy, nonlinear signals, thermal wave, thermal coupling, piezoelectric coupling, excess carrier coupling, ceramics, dielectrics, piezoelectrics, semiconductors.

Address for correspondence:
L.J. Balk, Universität Duisburg, Fachgebiet Werkstoffe der Elektrotechnik
Kommandantenstraße 60
4100 Duisburg 1,F.R.G. Phone No. (0203) 379 3407

Introduction

In scanning electron acoustic microscopy (SEAM) /3,4,10-13/ a primary electron beam of a scanning electron microscope (SEM), periodically modulated in its intensity is used to generate acoustic waves within the specimen region close to the beam entry point. As the modulation frequencies used until now in experiments are fairly low, at the most up to several MHz, the resulting acoustic wavelengths are in the order of mm or even longer /17/. Therefore, besides very crude specimen conditions, the propagation properties of the electron acoustic signal can be neglected, and only the generation of the acoustic signal itself plays a role in the formation of SEAM image contrast.

Thus the sound generation mechanism is the key to the understanding of SEAM micrographs. Up to now one possible mechanism has been discussed in detail, which is referred to as the thermal wave approach /18/. This is an intermediate production of thermal waves due to the energy dissipation of the primary electrons and a subsequent transposition of these thermal waves into elastic waves via the thermal expansion coefficient. Though this approach undoubtedly gives a correct description for many materials, for instance for many metals, it seems to fail - at least from experimental evidence /4/ - for many other solids of important interest such as ceramics, dielectrics, piezoelectrics and semiconductors. Furthermore, one has to consider that the deposition of the primary electron energy within the probed specimen region occurs in a very inhomogeneous manner /2/ and that, especially close to the center of the energy dissipation volume, there are regions of extremely high energy dissipation density. Due to these strong excitations, generation of nonlinear effects may occur /5,8/, as observed experimentally for most materials, which means a generation of harmonic, especially second harmonic signals. By means of these nonlinear signals, an even more sensitive evaluation of many material parameters can be observed with an even higher spatial resolution.

In the following an attempt is undertaken to interpret the experimental data obtained for different types of materials. Three different models, one being the known thermal wave approach,

are introduced and discussed in a similar and comparative manner in order to understand the SEAM micrographs gained for the corresponding materials.

The three stated mechanisms - thermal, piezoelectric and excess carrier coupling - are then corroborated experimentally for specific types of materials, where these sound generation processes turn out to be dominant.

List of symbols

s_T temperature induced strain
z coordinate normal to specimen surface
u particle displacement
α thermal expansion coefficient
T temperature rise above a starting temperature T_0
σ_T temperature induced stress
E_{el} elastic modulus
σ_M mechanically created stress
ρ_{cr} material density
v longitudinal sound velocity
s_M mechanically induced strain
σ total stress
K thermal conductivity
C_{th} specific heat
d_T thermal diffusion length
ω modulation frequency
d thickness of the specimen
n total excess concentration
n_a concentration of absorbed electrons
n_e concentration of generated electrons
n_p concentration of generated holes
g generation rate of excess carriers
τ_e lifetime of electrons
τ_p lifetime of holes
ρ electric space charge density
q quantum of electronic charge
E electric field
ϵ_0 permittivity of vacuum
c elastic stiffness constant
s total strain
e piezoelectric stress constant
F free energy per volume unit
S entropy per volume unit
ζ chemical potential per volume unit
D charge displacement
ϵ total permittivity
F_0 free energy per unit volume without applied electric field
a constant

General experimental conditions

The experimental arrangements described until now are very similar to each other /3,10,12/. The authors of this paper optimized the amplification of the acoustic signal by means of very versatile signal processing /3/. Both lock-in amplifiers and boxcar averagers are used to analyse the generated SEAM signal, thus allowing phase monitoring and determination of the actual temporal response of the acoustic wave. Fig. 1 gives a comprehensive block diagram of the set-up, which can be used for periodic, i.e. square wave operation and for detection at different harmonics.

There was no need for a special specimen preparation. Only the InP sample had been coated with a 30nm thick gold layer in order to prevent charging. The typical beam currents at the specimen ranged between about 10^{-7} A and 10^{-8} A for all measurements.

Models for generating sound by means of electron beams

The sound generation mechanism has previously been explained by means of a conversion of a periodic heat distribution into elastic waves due to the thermal expansion coefficient /17,18/. Though this so-called thermal wave approach is certainly one important mechanism, there is significant evidence from the author's experimental results, gained for a large variety of different material groups, that this thermal coupling process is not the only possible mechanism. Furthermore, it sometimes becomes negligible compared to other mechanisms involved. Two other important sound generation mechanisms are piezoelectric coupling in any piezoelectric material and excess carrier coupling in any semiconductor. These two material groups are very important in today's technology.

This section will give a presentation of the three coupling mechanisms mentioned in a comparative manner, pointing out the similarities and the differences of the three models. Therefore it is divided into three sections of identical structure, in which the model is introduced and experimental evidence in support of the model is presented.

Although the models are only treated one-dimensionally in order to allow a comparative discussion of all three mechanisms, they show those principal differences of the various coupling processes which actually are measured by the experiment.

For the following calculations some simplifying assumptions are made:

(i) isotropic medium,
(ii) semiinfinite solid state (in positive z-direction),
(iii) homogeneously distributed beam energy at specimen surface,
(iv) homogeneous energy dissipation at specimen surface, and
(v) uniform energy dissipation at specimen surface.

Thermal coupling

This mechanism takes into account a sound generation by electron beams due to heat production and thus an intermediate generation of thermal waves. Though this model was already treated more sophisticatedly (see for instance /13/), it is presented here in a comparative manner to the two other coupling mechanisms.

Model: In order to calculate the amplitude of the sound waves the temperature distribution in an elastic medium caused by the electron impact has to be evaluated.

The periodic temperature variation due to the modulated primary electron beam current I(t) is converted into stress waves via the thermal expansion of the material. The amplitude of these waves is dependent on the elastic status of the

specimen surface /22,23/.

Due to assumptions (i) and (iii)-(v) only longitudinal modes are considered. For the induced strain S_T one gets:

$$S_T = \left(\frac{\partial u(z,t)}{\partial z}\right) = \alpha T(z,t) \qquad (1)$$

with $u(z,t)$: z-component of particle displacement,
α : linear thermal expansion coefficient,
$T(z,t)$: temperature variation starting from an initial temperature T_0,
t : time.

Due to uniformity in the x- and y-directions, other components vanish. The resulting stress σ_T is:

$$\sigma_T = -E_{el}\alpha T(z,t) \qquad (2)$$

with E_{el} : elastic modulus.

This stress is completed by the mechanically created stress σ_M:

$$\sigma_M = \rho_{cr} v^2 s_M \qquad (3)$$

with ρ_{cr} : material density,
v : longitudinal sound velocity.

The total stress σ is given by:

$$\sigma = \rho_{cr} v^2 s_M - E_{el}\alpha T(z,t) \qquad (4)$$

From this the equation of motion for a particle in this region is given by:

$$\frac{\partial^2 u}{\partial t^2} = v^2 \frac{\partial^2 u}{\partial z^2} - \frac{\alpha E_{el}}{\rho_{cr}} \frac{\partial T(z,t)}{\partial z} \qquad (5)$$

with $u(z,t)$ not only being the local particle displacement, but also the measured acoustic quantity, too, when z is set to the thickness d of the specimen. The meaning of this final equation, which describes the sound generation process in general, is schematically sketched in fig. 2.

To a first approximation the temperature distribution $T(z,t)$ directly corresponds with the primary electron energy dissipation, not taking into account the energy dependence of different energy loss cross sections such as X-ray emission or Auger electron production. Therefore a numerical solution of eq. 5 can only be gained by precise knowledge of those energy dissipation processes leading to heat production. If the density of energy dissipation being transferred into heat is not too high, a separate solution of the heat conduction equation from the solution of eq. 5 is possible.

For high energy dissipation density, as is the case close to the center of the energy dissipation volume, both differential equations have to be solved together. In addition the temperature dependence of the expansion coefficient has to be considered. Both corrections may lead to the generation of higher harmonic signals.

As the temperature distribution $T(z,t)$ depends on the thermal conductivity K and the specific heat C_{th} of the specimen,too, the resulting thermal diffusion length (i.e., within a 1/e-decay of the temperature occurs) can be expressed by:

$$d_T = \left(\frac{2K}{\omega \rho_{cr} C_{th}}\right)^{1/2} \qquad (6)$$

with ω being the frequency of electron beam modulation. In three dimensions this quantity expresses approximately a sphere with radius d_T, in which generation of acoustic signals takes place due to the conversion of thermal into elastic waves. Thus the spatial resolution attained by SEAM due to thermal coupling should show a $\omega^{-1/2}$-dependence for the linear images.

For the thermal coupling it is worthwhile to mention that (compare eq. 5) the energy dissipation density is important for the quantity of the term $\partial T/\partial z$ and not the totally absorbed energy. Therefore changing primary electron beam parameters without varying the density of dissipation should not affect the acoustic signal amplitude, as,for instance,lowering the primary energy should not lead to a decreasing signal, as the penetration depth of primary electrons becomes smaller for lower energies.

Finally, in semiconducting material a treatment of thermal coupling, as usually done, is not allowed, because the heat production is not only

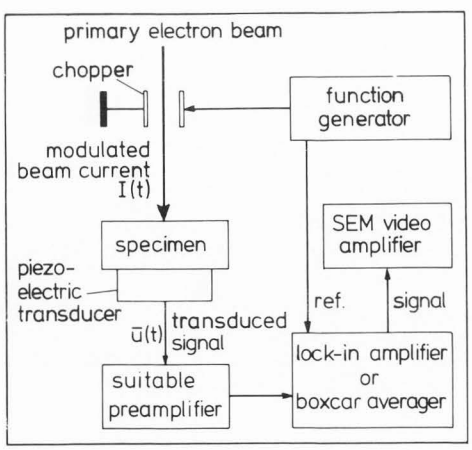

Fig. 1: Principal experimental arrangement

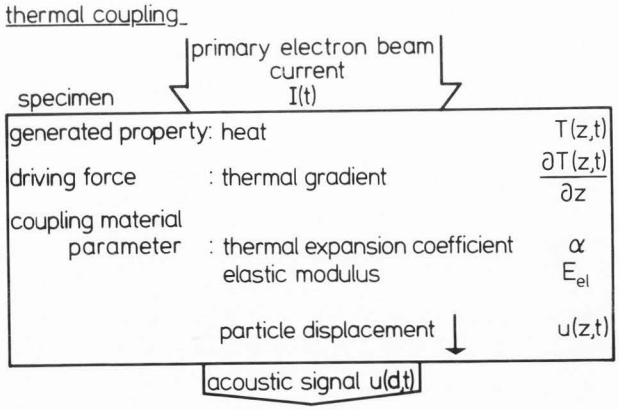

Fig. 2: Parameters important for thermal coupling

due to primary electron energy dissipation but also to excess carrier recombination. Therefore the heat production itself cannot be treated as being instantaneous any longer /20/. This assumption is not exact for the direct heating through the electron beam irradiation either, yet the time scale in which the heating occurs in this case is much smaller compared to the lifetimes of the generated excess carriers

Primary electrons of,for example,30keV typically produce about 10^4 electron-hole-pairs within the dissipation volume per one single primary electron. This enormous number of excess carriers undergoes a diffusion process first before recombining. As this diffusion is relatively slow, as there is a delay for the recombination ,and as the recombination process itself produces heat by means of nonradiative recombinations, a strong contribution of this mechanism to heat production is present, but with a different temporal behaviour than the direct heat production by primary electrons. Therefore, even if thermal coupling in a semiconductor would contribute to the SEAM signal, this signal generation would be strongly affected by the properties of the excess carriers such as diffusion length and carrier lifetime.

Furthermore, the spatial resolution should increase with the order of harmonic signals used, as it should be possible to generate these signals only in regions of extremely high energy density and thus close to the center of the energy dissipation volume. Moreover, the $\omega^{-1/2}$-dependence should not show up in the same manner as for linear signals, at least not in the frequency range used up to now.

Experimental evidence: Thermal coupling is certainly dominant for most metals. In these cases there is experimental evidence which directly backs the thermal wave approach.

The dependence of the spatial resolution on the modulation frequency in the linear mode is perfectly met for a large frequency range from about 50Hz up to more than 20MHz /6/, about six orders of magnitude in frequency.

There is no significant change of signal level for properly adjusted operating conditions when changing the primary electron energy. Though the actual power deposition is lowered by the reduced high voltage of the cathode, the penetration of the primary electron beam into the material diminishes simultaneously. Therefore the power dissipation density - to a first crude approximation - remains constant, at least it does not decrease. Fig. 3 shows two SEAM micrographs of a Cu-Zn-Al-alloy taken with primary energies of 25keV (beam current 1.3×10^{-7}A) and 10keV (beam current 1.5×10^{-7}A) with about identical signal level. This corroborates the dependence of u(d,t) on the power density rather than the total power /6/.

In the same manner operation at higher harmonics in the nonlinear modes should be weighted more closely to regions of high energy dissipation density. As this dissipation function is inhomogeneous, this effect would consequently lead to a higher spatial resolution in harmonics. As the generation rate of such nonlinear signals for usual measuring conditions is low and as the signal itself is weak, one could explain why not all specimen features can be recovered in the nonlinear images. However the strong contrast and the resolution limit in the nonlinear mode of the order of better than 1µm for metals even for low modulation frequencies and thus far beyond the linear SEAM image resolution under identical operation conditions /8/ stand opposite to such a mechanism.

Therefore it is more likely that specific nonlinear mechanisms (such as e.g. the proposed hysteretic, periodic shrinkage and growth of martensites in Cu-Zn-Al: D.G. Davies, from his Ph.D. Thesis, Cambridge Univ., U.K., Personal communication) cause a generation of nonlinear signals in metals.

Piezoelectric coupling

This mechanism involves the sound production due to piezoelectricity within the material and an inhomogeneous electric field at the beam entry point.

Model: A primary electron beam generally produces an inhomogeneous excess charge within the dissipation volume in nonmetallic materials. This excess concentration n can be caused by two different mechanisms:
- local distribution of absorbed electrons (n_a), and
- generation of electron-hole-pairs (n_e,n_p).

As for most piezoelectric materials the electronic band gap is not much larger than in semiconductors (barium titanate and zinc oxide have band gaps of about equal value) and as many semiconductors have an additional piezoelectric behaviour, the second mechanism is treated in the calculation only because of its major technical importance. Nevertheless the results obtained just with absorbed electrons give the same principal results.

The generated excess carrier concentrations n_e,n_p are given by:

$$n_{e,p} = g(\underline{r})\tau_{e,p} \qquad (7)$$

with $g(\underline{r})$: generation rate of excess carriers (depending on material properties, beam parameters and distance to the beam entry point /24/),
τ_e : lifetime of electrons
τ_p : lifetime of holes.

The excess carriers diffuse away from their location of generation due to the concentration gradient. Caused by different lifetimes /4/ a space charge region is created /2/. This space charge $\rho(\underline{r})$ can be expressed by:

$$\rho(\underline{r}) = -q\{n_e(\underline{r}) - n_p(\underline{r})\} = -qg(\underline{r})(\tau_e - \tau_p) \qquad (8)$$

with q as the quantum of electronic charge.
The charge distribution creates an electric field $\underline{E}(\underline{r})$ /9/:

$$\underline{E}(\underline{r}) = \frac{1}{4\pi\varepsilon_0} \iiint_V \rho(\underline{r}) \frac{\underline{r} - \underline{r}'}{|\underline{r} - \underline{r}'|^3} d^3\underline{r}' \qquad (9)$$

when ε_0 is the permittivity of vacuum.

The electric field stresses the lattice in a piezoelectric medium. One-dimensionally /16/ the resulting strain is:

$$\sigma = cs - eE \qquad (10)$$

with c : elastic stiffness constant,
s : strain and
e : piezoelectric stress constant.
The equation of motion is again given by:

$$\rho_{cr} \frac{\partial^2 u}{\partial t^2} = \frac{\partial \sigma}{\partial z} \qquad (11)$$

By expressing the particle displacement u(z,t) by strain and electric field, one gets:

$$\frac{\partial^2 u}{\partial t^2} = \frac{1}{\rho_{cr}} \left(c \frac{\partial s}{\partial z} - e \frac{\partial E}{\partial z} \right) \qquad (12)$$

and with the strain s expressed by:

$$s = \frac{\partial u}{\partial z} \qquad (13)$$

the final equation results:

$$\frac{\partial^2 u}{\partial t^2} = v^2 \frac{\partial^2 u}{\partial z^2} - \frac{e}{\rho_{cr}} \frac{\partial E(z,t)}{\partial z} \qquad (14)$$

This equation has the same form as eq. 5 for the thermal coupling. The parameters important for acoustic signal generation for piezoelectric coupling are sketched in fig. 4.

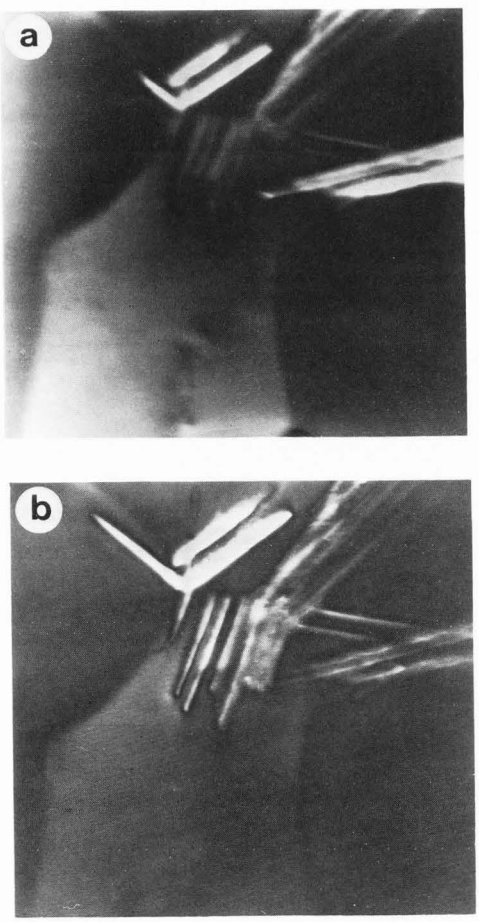

Fig. 3: Linear SEAM amplitude images of Cu-Zn-Al alloy taken at different primary energies. Operation frequency: 189kHz; a) 25keV, b) 10keV

100µm

From this easy model one can realize already that for this coupling mechanism the energy dissipation density is the important quantity, as the variation of the electric field strength is directly dependent upon the concentration of excess charge density. Whereas this dependence on the dissipation density is similar in thermal coupling, in piezoelectric coupling no pronounced frequency dependence of the spatial resolution should occur in the frequency range under present investigation. The maximum volume being responsible for the sound generation should be the primary energy dissipation volume slightly enlarged by the carrier diffusion length, which in most cases is in the order of 1...5µm and thus somewhat smaller than the typical diameter of the dissipation volume for most piezoelectric materials (assuming 30keV primary energy).

As the piezoelectric coupling is a linear effect, it has to be expected that a change of electric polarities changes the sign of the generated acoustic amplitude, too, which necessarily causes a phase shift of 180° of the acoustic wave.

The above calculations are only valid for low energy densities. Again close to the center of the dissipation there may be dissipation densities, which can cause nonlinear effects. The spatial resolution for nonlinear signals should increase again, but not in the same order of magnitude as for metals, as here the carrier diffusion becomes the limiting factor. However, it seems more likely that for this generation mechanism, only specific nonlinear mechanisms besides piezoelectric coupling would contribute strong nonlinearities to the electron acoustic signal, too.

Experimental evidence

If piezoelectric coupling is dominant (or at least plays an important role in the acoustic signal generation), there should be no frequency dependence of the spatial resolution in the same order of magnitude as for thermal coupling. Therefore the spatial resolution should be in the order of the resolution for secondary electron images. This could be realized for any piezoelectric material examined by the authors. Furthermore, a change of magnitude or direction of the

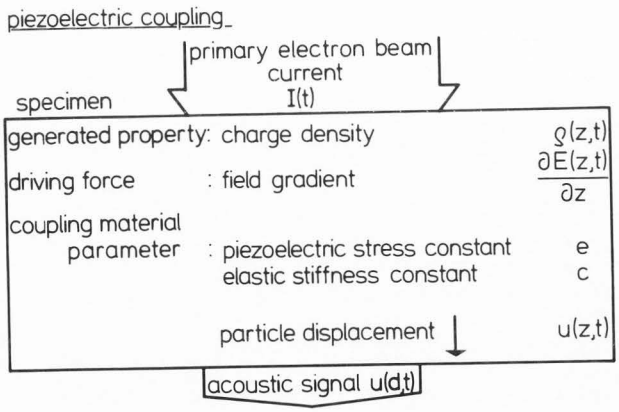

Fig. 4: Parameters important for piezoelectric coupling

piezoelectric stress moduli should be revealed by a corresponding contrast in the SEAM image. Fig. 5 is such a linear SEAM micrograph of a polished, nearly perfect barium titanate single crystal of homogeneous properties (barium titanate is strongly piezoelectric: $0.2C/m^2$) with a tetragonal symmetry. The only structures to be seen - besides some specimen damage in the bottom left corner - are ferroelectric domains arranged in a regular manner, which could be imaged also by the voltage contrast method.

Both the possibility of detecting those domains, as can be shown for barium titanate ceramics, too (compare fig. 6), and the apparent high spatial resolution of better than 1µm do not allow the application of the thermal coupling model for this material, but can be interpreted well by piezoelectric coupling.

In the case of a strong piezoelectric coupling mainly a linear dependence of the signal on the electric field induced by the primary electron beam and therefore only linear SEAM images should be detectable with reasonable signal levels, which is the case for the experiments carried out until now.

Changing electric polarities changes the sign of the acoustic signal, as already stated in the theoretical part of this section. In indium phosphide (InP: $0.04C/m^2$ /1/) this statement could be proven precisely, as the phase of the acoustic wave switches at any pn-junction by 180° due to the sign inversion in the p-region with respect to the n-region. This sign inversion occurs at the precise position of the pn-junction /3/ (compare the following discussion of the InP results in the section on excess carrier coupling).

In indium phosphide as a piezoelectric semiconductor the sound generation is due to both piezoelectric and excess carrier coupling. Once a sound wave is produced within this material, it simultaneously generates an alternating electric field due to its piezoelectric properties. This field then overlaps the other electric fields in a semiconductor such as the field of the penetrating electron beam and of locally existing fields of pn-junctions. Especially the coupling between these junction fields and the high frequency crystal fields leads to polarity effects, and, if tuned to high enough frequencies, to local amplification of the acoustic signal (fig. 7). This amplification should be polarity dependent, as piezoelectric coupling is linear and hence, if the electron beam scans from p- to n-regions should give a reversed sign of signal as compared to the beam scanning from n- to p- /3/. This is demonstrated in fig. 8a. Additionally, in this material anytime electrostriction is present, and as the piezoelectricity in InP is not too pronounced, a detection of second harmonic signals is possible /3/. The nonlinear mode therefore should lead to the same resonances at the pn-junctions, but without a sign inversion due to the E^2-dependence of electrostriction. This - within the limits of experimental quality - can be recognized in fig. 8b taken with identical parameters as the linear image of fig. 8a.

In any case such a polarity dependence of SEAM images - both for amplitude and phase behaviour - is unexplainable by means of thermal coupling. Again here a spatial resolution is gained which is better than should be expected by thermal coupling. Changing from linear to nonlinear images does not give such significant changes in resolution as possible in metals, which is in coincidence with the lack of an intermediate thermal wave region.

Excess carrier coupling

This coupling considers sound generation through excess carrier generation via the deformation dependent tensor of permittivity.

Model: As the primary electrons produce an electric field within the dissipation volume, as already treated in the previous section, there occurs a change of the free energy per volume unit within a dielectric medium. This free energy change is given, as is well known by thermodynamics, by /15/:

$$dF = -SdT + \zeta d\rho_{cr} + \frac{1}{4\pi} EdD \qquad (15)$$

with F : free energy per volume unit,
S : entropy per volume unit,
ζ : chemical potential per volume unit, and
ρ_{cr} : material density.

Using the variable:

$$\overline{F} = F - \frac{1}{4\pi} ED \qquad (16)$$

one gets:

$$d\overline{F} = -SdT + \zeta d\rho_{cr} - \frac{1}{4\pi} DdE \qquad (17)$$

Integration of this equation for a nonpyro- and nonpiezoelectric material yields:

$$\overline{F} = F_o - \frac{1}{8\pi} \epsilon E^2 \qquad (18)$$

with $D=\epsilon E$.

For small values of strain:

$$s = \frac{\partial u}{\partial z} \qquad (19)$$

the deformation dependent permittivity of the material becomes:

$$\epsilon = \epsilon_o + as \qquad (20)$$

with a=const..

For an isothermal variation of the thermodynamical state (dT=0) one gets for a small variation of $\overline{F}$ /15/:

$$\delta\overline{F} = -\frac{1}{4\pi} D\delta E + \frac{\partial\overline{F}}{\partial s} \delta s \qquad (21)$$

According to /15/ the stress tensor can be written as:

$$\sigma = \overline{F} + \left(\frac{\partial\overline{F}}{\partial s}\right)_{T,E} + \frac{1}{4\pi} ED \qquad (22)$$

and with the expression already given for $\overline{F}$:

$$\sigma = \sigma^o + \frac{1}{8\pi} (\epsilon_o - a) E^2 \qquad (23)$$

and thus the final equation:

$$\frac{\partial^2 u}{\partial t^2} = v^2 \frac{\partial^2 u}{\partial z^2} + \frac{\varepsilon_0 - a}{8\pi\rho_{cr}} \frac{\partial E^2(z,t)}{\partial z} \qquad (24)$$

Material properties and beam parameters being important for excess carrier coupling are schematically shown in fig. 9.

Though of the same structure as the preceding eq. 5 and eq. 14 an important difference has to be noticed to thermal and piezoelectric coupling, which is that this excess carrier coupling in

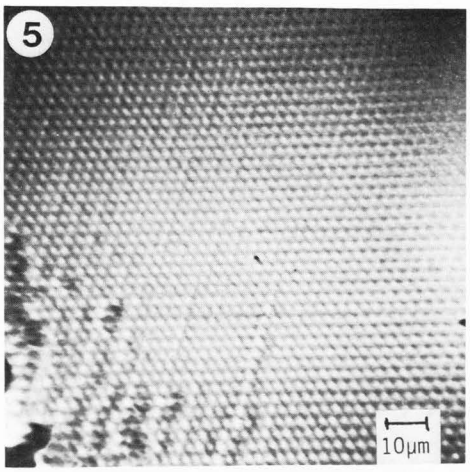

Fig. 5: Ferro-electric domains visible by linear SEAM amplitude micrograph; modulation frequency: 100kHz; primary electron energy: 30keV.

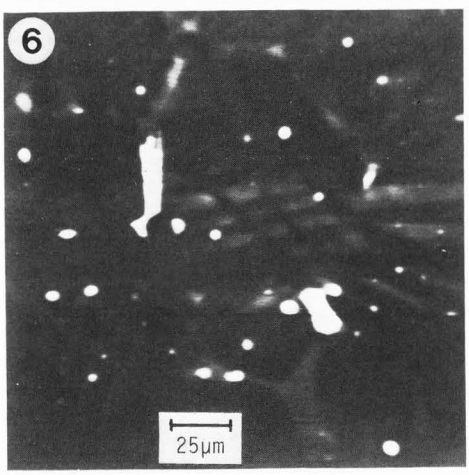

Fig. 6: Grain and domain structure in linear SEAM amplitude image; modulation frequency: 100kHz; primary electron energy: 30keV.

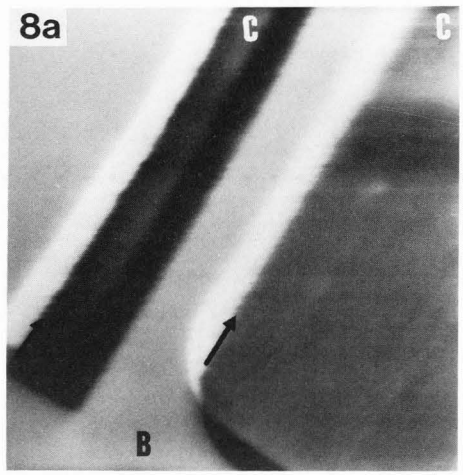

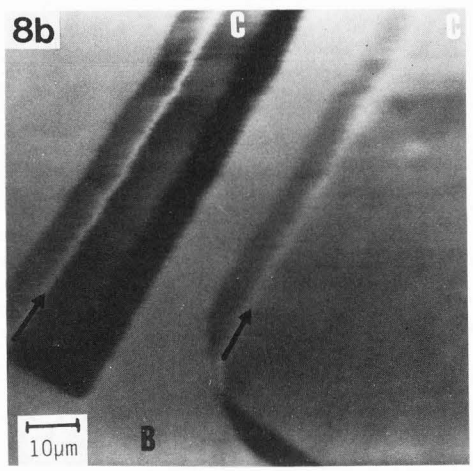

Fig. 8: Electron acoustic response of pn junctions in InP. Information: Axsin (Ø) with A amplitude and Ø relative phase position of acoustic wave with respect to modulating waveform (compare /3/); modulation frequency: 10MHz; primary electron energy: 5keV; a) linear image; b) nonlinear second harmonic image; B, undoped, C, doped regions; arrow, pn-junction.

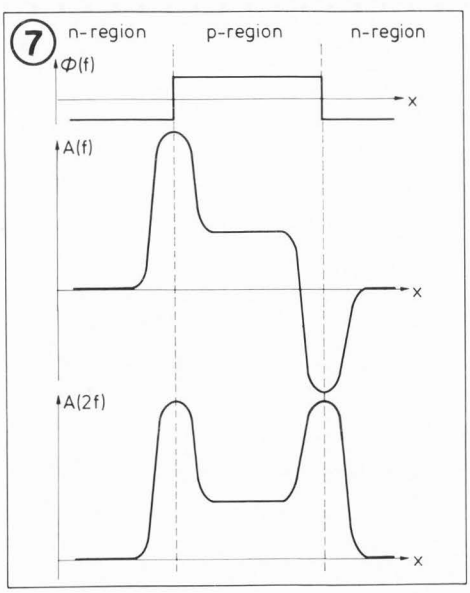

Fig. 7: Interpretation of SEAM images of selectively doped InP for high frequencies.

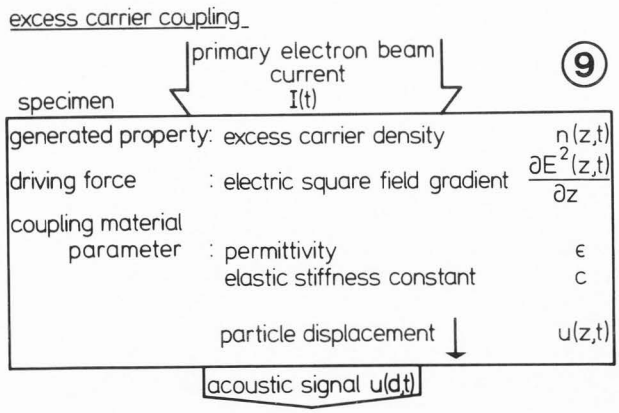

Fig. 9: Parameters important for excess carrier coupling

principle occurs nonlinearly due to a dependence of the generation on $\partial E^2/\partial z$. Therefore interpretation of second harmonic SEAM images in non-piezoelectric semiconductors should be optimum in terms of semiconductor properties.

In spite of the square dependence on the electric field a similar behaviour of excess carrier coupling as for piezoelectric coupling has to be expected, that means a comparable spatial resolution, as a similar sound generation volume has to be considered (primary electron energy dissipation enlarged by excess carrier diffusion). There should be no significant change of spatial resolution with modulation frequency like in metals for the frequency range used up to now. And again the density of dissipation is important and not the totally deposited energy.

Experimental evidence: If excess carrier coupling occurs, any process which is involved in the production of excess carriers should show the same spatial resolution and should be a competitive signal generation mechanism to SEAM. This is in excellent agreement with the experiments, as the resolutions gained by SEAM, electron beam induced current (EBIC) and cathodoluminescence (CL) obtained for the same specimens are identical to each other. This statement holds both for silicon /19/ and compound semiconductors (Löhnert K.: private communication). Especially dislocation lines have shown the same resolution in CL and SEAM /3/. As this correlation of spatial resolution occurred in every reported experiment (for InP /3/, GaAs /19/, silicon devices /4/ and polycrystalline silicon /19/), it is very unlikely that thermal properties can explain this coincidence between the three signals of SEAM, EBIC and CL.

If excess carrier coupling is important, any locally existing electric field must diminish the SEAM amplitude, as within this material region the generated excess carriers are separated by the electric field and thus contribute to an internal, quite often non-detectable EBIC generation (especially for polycrystalline material).

Thus the SEAM micrograph should reveal regions of such existing fields like at any pn-junction or similar electric barrier, for instance at boundaries of grains of different doping levels. Already potential barriers of about 0.1eV are strong enough to give a satisfactory separation of excess carriers and a pronounced internal EBIC generation /2/. This phenomenon is proven by the examination of InP device structures, where there is a mismatch of the actual doping structure with the SEAM results by just the order of a minority carrier diffusion length, which is in agreement with the model of excess carrier coupling. That means that the SEAM amplitude rolls off in the same manner as a noticeable internal EBIC signal comes up (as is well known for p-n junctions). This statement holds true only for lower frequencies for InP, at higher frequencies a coupling with the alternating field of the acoustic wave occurs (compare previous section on piezoelectric coupling). The low frequency signal situation for this type of piezoelectric and semiconducting material is sketched in the diagram of fig. 10 /3/.

It should be noted that the phase variation of SEAM gives directly the doping profile, whereas the amplitude signals are affected by the existing electric fields of different frequencies in this material.

Fig. 11 is a comparison between a SEAM image of InP device structure already taken with a modulation frequency of several MHz and the secondary electron image, which directly correlates to the actual doping structure (concentrations - doped: $10^{18}cm^{-3}$, undoped: $10^{16}cm^{-3}$). One easily can see the mismatch of about 8µm, which is twice the approximate value for the minority diffusion length in this material (Schmitt R.: private communications) and which clearly reveals the existence of the electric field around the junction, as this mismatch can be traced at any location within this micrograph.

In non-piezoelectric materials like silicon the nonlinear signals at the second harmonic should be present even for low excitation conditions, which could be shown for polycrystalline silicon /5/. Furthermore, it should give a contrast with explainable structures, whereas the linear image should be a mixture of other signals, too, like some contribution from thermal coupling. Fig. 12 shows a section of this material, in which the actual grain boundary shows up black, that means that there is no SEAM signal. This is in coincidence with the discussion in the previous paragraph, as there is typically an electric barrier present at the boundary due to different doping levels /21/, causing a creation of internal EBIC signals which are in competition with SEAM.

The neighbouring white regions on both sides of the grain boundary are very typical for this material and are due to regions of strongly decreased carbon and oxygen content, so-called ´denuded zones´ /21/.

Carbon and oxygen do not change the electronic properties of silicon to a first approach, but similar to carbon in steel they change the stiffness of the material. As excess carrier coupling occurs, the driving force due to the electron beam impact remains constant, whereas due to the lower stiffness of the material in the denuded zones compared to the grain volume the resulting particle displacement and thus the SEAM signal are increased. These results are backed by etching techniques revealing regions of changed carbon and oxygen content.

Again variation of the operation frequency up to several MHz does not show a pronounced change in the obtained spatial resolution. Furthermore, the SEAM resolution in silicon, both obtained by the authors and others /19/, are much better than those values predicted from thermal wave theory. Whereas already for 100kHz operation values of better than 1µm are typical, the theoretical value for even 1MHz operation is only 5µm /19/. To support this, in InP even resolution values of about 0.2µm are recorded for 100kHz operation /3/.

Conclusions

In this paper three different models for the generation of acoustic signals are discussed in comparison to show that depending on the material

properties different processes become dominant. All three models, though treated very simply and one-dimensionally give a first and, as shown by the discussed experiments, reasonable description of the physical processes involved. For the materials discussed a dominance of one coupling mechanism was given (with the exception of InP, where two processes have to be considered). For arbitrary materials, however, an experimental procedure is not yet developed, which would allow a definite determination of the relative strengths of the mechanisms involved.

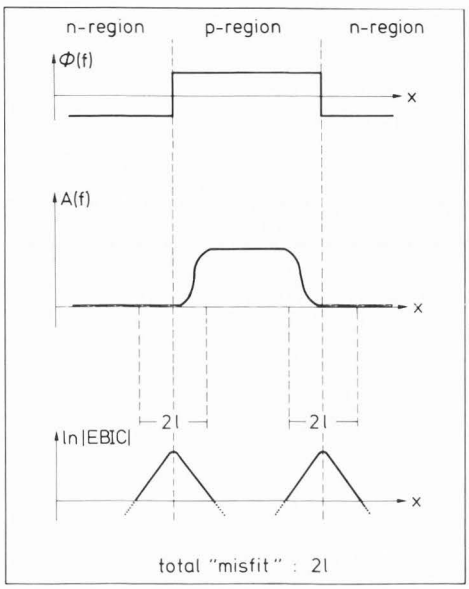

Fig. 10: Interpretation of SEAM images of selectively doped InP for low frequencies.

Furthermore, due to the complexity involved in solving the theoretical treatment, only one-dimensional calculations are carried out, which necessarily have to be extended into a three-dimensional treatment. This certainly gives a more realistic result and it will reveal other dependences of SEAM on material properties, such as shown already for the thermal coupling /13,14/. There a three-dimensional treatment enables the introduction of elastic properties in the SEAM image formation in addition to the thermal parameters.

The origin of the nonlinearities due to other effects than mentioned, as e.g. hysteretic effects of the material itself, is not treated at all. Finally, it should be emphasized that the coupling mechanisms mentioned are not the only ones possible. Evidence for this is the fact that it is easily possible by SEAM to detect ferromagnetic domains, an effect which might be due to

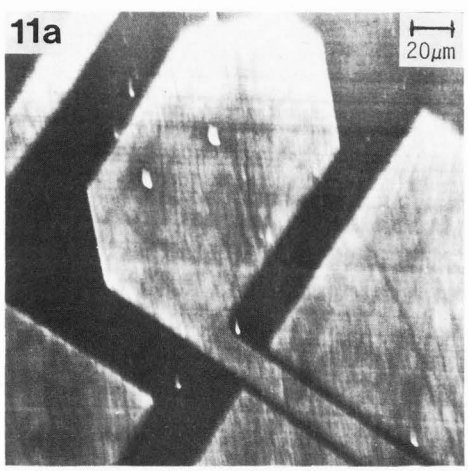

Fig. 11: Comparison of actual doping profile with SEAM micrograph a) secondary and backscattered electron image; b) linear SEAM micrograph taken at a modulation frequency of 5.6MHz; dark regions undoped; information Axsin (Ø).

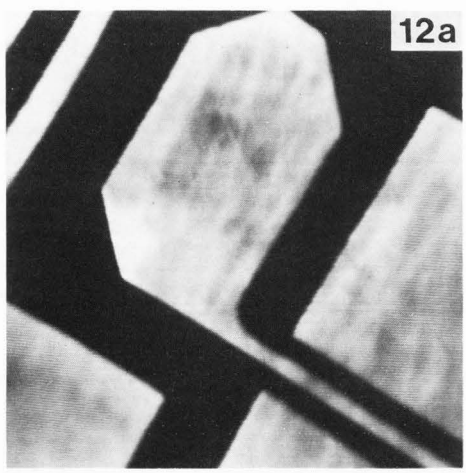

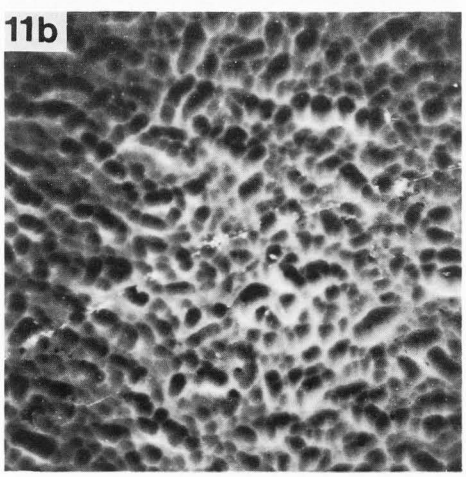

Fig. 12: Polycrystalline solar silicon; a) secondary and backscattered electron micrograph; b) second harmonic SEAM amplitude micrograph; primary electron energy: 30keV; modulation frequency: 100kHz.

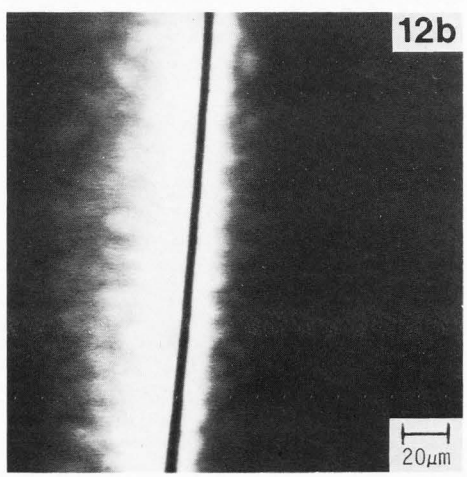

some kind of magnetic coupling /7/.

Therefore this paper can only be understood as a start into a more detailed and careful analysis of all physical processes contributing to the generation of SEAM signals. A task, which necessarily has to be done in order to optimize the operation parameters of this technique, its applicability and last but not least the possibility to interpret the micrographs obtained for the different types of materials and devices.

Acknowledgements

The authors would like to thank Prof. E. Kubalek for many helpful discussions. K. Löhnert assisted with discussions and experiments of EBIC and CL. D.G. Davies from Cambridge university took part in experiments for metals and some theoretical proposals.

References

/1/ Bachmann KJ. (1981), Properties, preparation and device applications of indium phosphide. Ann. Rev. Mater. Sci. II, 441-484.

/2/ Balk LJ, Menzel E, Kubalek E. (1977). Microcharacterization of semiconductors by cathodoluminescence (CL) and electron beam induced current (EBIC) techniques. 8th Int. Congr. X-ray Optics and Microanalysis, (ed.) D.R. Beaman et al., Pendall Publ. Co., Midland, MI. 613-624.

/3/ Balk LJ, Kultscher N. (1983a). Techniques for electron acoustic microscopy. Inst. Phys. Conf. Ser. 67, Sect. 8, 387-392.

/4/ Balk LJ, Kultscher N. (1983b). Scanning electron acoustic microscopy. BEDO 16, 107-120.

/5/ Balk LJ, Kultscher N. (1984). Nonlinear scanning electron acoustic microscopy. Journal de Physique 45 (2), C2-869 - C2-872.

/6/ Balk LJ, Davies DG, Kultscher N. (1984a). The dependence of electron acoustic microscopy (SEAM) imaging on chopping and detection frequencies for metal samples. Phys. stat. sol. (a) 82 (23), 23-33.

/7/ Balk LJ, Davies DG, Kultscher N. (1984b). Investigations of Si-Fe transformer sheets by scanning electron acoustic microscopy (SEAM). IEEE Trans. on Magnetics Mag-20 (5), 1466-1468.

/8/ Balk LJ, Davies DG, Kultscher N. (1984c). Application of nonlinear scanning electron acoustic microscopy in metals research. Scanning Electron Microsc. 1984; IV: 1601-1610.

/9/ Becker R, Sauter F. (1973). Theorie der Elektrizität 1. Teubner Verlag, Stuttgart, 9-13.

/10/ Brandis E, Rosencwaig A. (1980). Thermal wave microscopy with electron beams. Appl. Phys. Lett. 37 (1), 98-100.

/11/ Cargill III GS. (1980). Ultrasonic imaging in scanning electron microscopy. Nature 286, 691-693.

/12/ Cargill III GS. (1981). Electron-acoustic microscopy. Physics Today, October, 1981. 7-32.

/13/ Davies DG. (1983). Scanning electron acoustic microscopy. Scanning Electron Microsc. 1983; III: 1163-1176.

/14/ Holstein WL, Begnoche BC. (1984). Electron thermoelastic acoustic microscopy imaging of copper oxide particles on copper. Scanning Electron Microsc. 1984; III: 1033-1040.

/15/ Landau LD, Lifschitz EM (1980). Lehrbuch der theoretischen Physik VIII, Akademie-Verlag, Berlin, 57-96.

/16/ Mason WP. (1966). Physical Acoustics IV (A). Academic Press, New York, 1-19.

/17/ Opsal J, Rosencwaig A. (1982). Thermal-wave depth profiling: Theory. J. Appl. Phys. 53 (6), 4240-4246.

/18/ Rosencwaig A, Gersho A. (1976). Theory of the photoacoustic effect with solids. J. Appl. Phys. 47 (1), 64-69.

/19/ Rosencwaig A. (1984) Thermal wave imaging in a scanning electron microscope. Scanning Electron Microsc. 1984; IV: 1611-1628.

/20/ Sablikov VA, Sandomirskil VB. (1983). Theory of the photoacoustic effect in semiconductors. Sov. Phys. Semicond. 17 (1), 50-53.

/21/ Seiter H. (1983). Arbeitskreis "Punktdefekte in Silizium", Stuttgart.

/22/ Smirnow WI. (1977). Lehrgang der höheren Mathematik II. Deutscher Verlag der Wissenschaften, Berlin, 560-566.

/23/ White RM. (1963). Generation of elastic waves by transient surface heating. J. Appl. Phys. 34 (12), 3559-3567.

/24/ Wittry DB, Kyser DF. (1967). Measurements of diffusion lengths in direct-gap semiconductors by electron-beam excitation. J. Appl. Phys. 38, 375-382.

Discussion with Reviewers

W.L. Holstein: Do you observe vibrational patterns for those specimens where the generation of the acoustic force has been attributed to "piezoelectric coupling" and "excess carrier coupling" similar to those that you /4/ and others /12, 13, 14/ have reported when acoustic force generation occurs through "thermal coupling"?

Authors: Up to now it has not been possible to detect any structures that could be identified with vibrational patterns in those materials, where the generation of acoustic signals is attributed to piezoelectric or excess carrier coupling.

W.L. Holstein: In the derivation of equation (3) for "excess carrier coupling", you assume that temperature is constant. However, the periodic electron beam results in large periodic temperature variations. What effect do these temperature variations have on the derivation and application of eq. (3)?

Authors: Both the incident primary electrons and the generated excess carriers lead to a heat pro-

duction in the generation volume of the acoustic signal and thus to a spatial as well as a temporal temperature variation. If this dependence would be considered, too, the variation of the free energy would result in an additional term in the calculated stress depending on T. A quantitative evaluation for a special type of material at this time cannot be given, however, the intention of this paper is only to show the principal applicability of physical mechanisms other than thermal coupling to the generation of electron acoustic signals in materials important in today's technology. Furthermore, the experiments have shown that a qualitative interpretation of the measurements can well be done without considering this effect.

W.L. Holstein: Isn't the charge build-up from secondary electron emission much greater than that from carrier diffusion within the specimen?
Authors: Disregarding a special material one can say in general that for normal incidence (which is the usual case for the measurements) the number of secondary electrons is in the same order of magnitude as the number of primary electrons whereas a single primary electron will generate up to 10^4 excess carriers (at 30keV). Even if the lifetimes of electrons and holes are only slightly different the resulting field should be stronger than that due to secondary electrons. Nevertheless, the generation mechanism via piezoelectric coupling, as stated in the corresponding section of the paper, is not dependent upon what causes the driving electric field.

R. Huebener: I believe the statement of the authors that the harmonic signals are not expected to show the $\omega^{-1/2}$-dependence must be qualified somewhat. There is always a frequency range in which the skin effect for the excitation has to be taken into account. However, the characteristic frequency above which the skin effect with the $\omega^{-1/2}$-dependence is expected for the harmonic signals, is only shifted to much higher frequencies.
Authors: The frequency dependences of the EA signal due to the influence of the skin effect, piezoelectric coupling or heat production due to the electron beam irradiation are significant only beyond a much higher frequency compared to those usually used up to now. Therefore it seemed to be admissible to neglect the influences for a qualitative comparison of the three coupling mechanisms in SEAM addressed in the paper.

A.Rosencwaig: The claim that spatial resolution varies as $(\omega)^{-1/2}$ is incorrect. The thermal-wave imaging mechanism involves not simply the temperature but rather an average of the temperature and therefore the frequency dependence can be expected to be more like $(\omega)^{-1}$.

Other complicating issues have to do with the size of the beam relative to the thermal diffusion length and how far the feature being imaged is from the sample surface. When the distance of a feature from the surface and the size of the beam are both smaller than the thermal diffusion length the spatial resolution is independent of the modulation frequency.
Authors: Opposite to the opinion of the reviewer the authors cannot argue against experimental evidences which clearly show the stated $\omega^{-1/2}$-dependence of the image resolution between frequencies of 50Hz up to 50MHz for the thermal-wave mechanism.

Assuming the reviewer's suggestion, the resolution values for all images taken under normal experimental conditions, with features up to about 2µm beneath the surface should be independent of the modulation frequency, a feature being against the authors' experience.

A. Rosencwaig: As far as recombination effects on the heating are concerned, whether this is a faster or slower process depends on the modulation frequency.
Authors: This is a correct statement but it does not call in question the given arguments. The maximum of the relevant frequency is mainly determined by the carrier lifetimes. The frequencies used at present correspond quite often to typical charge carrier lifetimes.

A. Rosencwaig: No results seem to have been presented on metals which are new or refute the thermal wave imaging mechanism.
Authors: This paper represents a more theoretical treatment in which the experimental results of the authors (together with D.G. Davies) are combined in order to present the three discussed mechanisms. Taking into account the magnetic coupling, too, would contradict the thermal coupling even for metals as the only possible mechanism, as this does not provide a model for the observed magnetic contrasts.

A. Rosencwaig: The model for a space charge effect is certainly incomplete and oversimplified. When excess carriers undergo recombination the only charge remaining is that from the electron beam.
Authors: Both the space charge and the heating are transients. Therefore it depends on the time scale which effect becomes dominant.

A.Rosencwaig: Second harmonic signals can be produced very easily by over driving the electronics. This may be the origin of the author's observations. At the very least they should convince the reader that their observed nonlinearities are coming from the sample and are not some artifact of their detection and electronics system.
Authors: The question about the origin of the observed nonlinearities has already been answered extensively in the paper. Detailed measurements which definitely prove the given statements are presented in the PhD thesis of D.G. Davies.